Noise-stabilized random attractor

J. M. Finn,[1] E. R. Tracy,[2] W. E. Cooke,[2] and A. S. Richardson[2]
[1]*T-15, Plasma Theory, Los Alamos National Laboratory, Los Alamos, New Mexico 87545, USA*
[2]*Department of Physics, College of William and Mary, Williamsburg, Virginia 23187, USA*
(Received 8 March 2005; revised manuscript received 22 November 2005; published 23 February 2006)

A two-dimensional flow model is introduced with deterministic behavior consisting of bursts that become successively larger, with longer interburst time intervals between them. The system is symmetric in one variable x and there are bursts on either side of $x=0$, separated by the presence of an invariant manifold at $x=0$. In the presence of arbitrarily small additive noise in the x direction, the successive bursts have bounded amplitudes and interburst intervals. This system with noise is proposed as a model for edge-localized modes in tokamaks. With noise, the bursts can switch from positive to negative x and vice versa. The probability distribution of burst heights and interburst periods is studied, as is the dependence of the statistics on the noise variance. The modification of this behavior as the symmetry in x is broken is studied, showing qualitatively similar behavior if the symmetry breaking is small enough. Experimental observations of a nonlinear circuit governed by the same equations are presented, showing good agreement.

DOI: 10.1103/PhysRevE.73.026220 PACS number(s): 05.45.−a, 05.40.−a, 02.50.Ey, 05.10.Gg

I. INTRODUCTION

This paper is motivated by observations of extreme noise sensitivity in a two-dimensional flow of the form

$$\frac{dx}{dt} = f(x,y) \equiv (y-1)x, \tag{1}$$

$$\frac{dy}{dt} = g(x,y) \equiv \epsilon y^{\nu} - x^2 y. \tag{2}$$

This system is a low-dimensional model for the nonlinear behavior of a plasma instability in which y represents the pressure gradient, and instability (with amplitude x) is driven by the pressure gradient and fixed magnetic field line curvature. Such pressure-driven instabilities are thought to be responsible for edge-localized modes (ELMs) observed as fluctuations at the edge of a tokamak [1,2]. Some ELMs, called type-I ELMs, show temporal behavior which is quite simple, consisting of well separated large bursts, indicating that their dynamics can be represented by a low-order system. However, the time series appear to show chaos, and it is of some interest to determine whether this apparently chaotic behavior is indeed deterministic chaos or whether it is due to sensitivity to noise from, for example, the plasma core. For example, if the apparent chaos is due to noise, the behavior can occur in a two-dimensional model, whereas an autonomous model showing similar apparently chaotic behavior must be at least three dimensional.

The effect of noise has been studied in other experimental physics situations, and the kind of extreme sensitivity to noise we discuss here has been observed. For example, in experiments involving the formation of droplets in a viscous fluid [3], the fluid is observed to form thin necks repeatedly as a part of the process. Simulations showed the formation of necks, but the *repeated* formation of necks required noise in the modeling, although extremely small noise gave agreement. Another example involves studies of a neodymium-doped yttrium aluminum garnet laser with an intercavity potassium titanyl phosphate crystal. Theoretical studies were performed to model the laser dynamics [4], showing that the type-II chaotic dynamical behavior of the laser was observed to be very sensitive to noise and was actually found to amplify the noise. Because of the role of a very low level of noise in such disparate physical systems, we have been motivated to do detailed studies of (1) and (2) and related systems perturbed with a low level of noise.

For the system (1) and (2) with zero noise, the behavior ϵy^{ν} arises for the following reason: on time scales longer than the time for magnetic flux to penetrate the edge region, the electric field equals the driving field E and Ohmic heating takes the form $\partial T/\partial t \sim \sigma E^2$, where T is the electron temperature and $\sigma \sim T^{3/2}$ is the electrical conductivity. This gives $\partial T/\partial t \sim T^{3/2}$ (until the growth is limited by thermal conduction) and the pressure gradient y is proportional to T. Then the magnetic field x grows if $y>1$, but for large enough field x the term $-x^2 y$, which represents the flattening of the pressure gradient due to the fluctuation, enters. This causes a decrease in y, which quenches the growth of x. Other bursty behavior observed in plasma devices, for which the amplitude and characteristic period may be related to noise, include sawtooth oscillations in tokamaks and reversed field pinches.

For this flow, $x=0$ is an invariant manifold, the unstable manifold of the fixed point at $x=y=0$. See Fig. 1. The x axis is the stable manifold of the same fixed point. There are two unstable spirals with $x=\pm x_0=\pm\sqrt{\epsilon}$. The nonlinear deterministic behavior consists of orbits coming out of these spirals, with increasingly larger bursts more widely separated in time. Because of symmetry in x, identical bursts can occur on both sides of $x=0$, isolated from each other by the invariant manifold $x=0$.

With a small amount of uncorrelated Gaussian noise added to Eq. (1), we find that the resulting nonlinear stochastic equation has the following property: the bursts saturate in amplitude, leading to behavior that is qualitatively similar to deterministic chaos. We call this behavior *noise stabilization*. Further, the noise allows transitions across the y axis, an

 ©2006 The American Physical Society

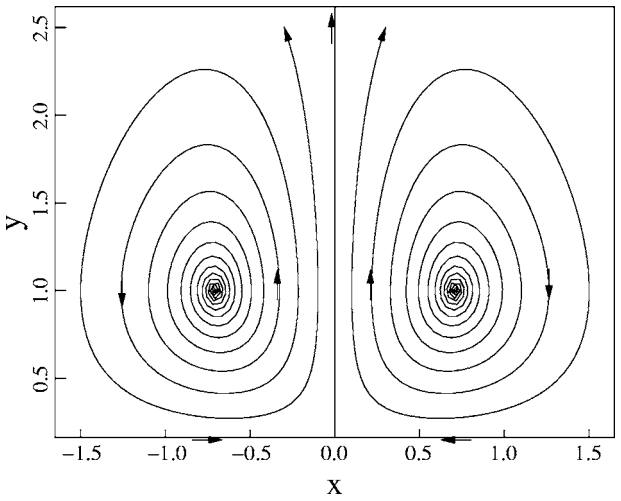

FIG. 1. Orbits initiated near the fixed points at $x=\pm x_0=\pm\sqrt{\epsilon}$, $y=1$. The orbit on the right spirals out clockwise, the one on the left counterclockwise. The x and y axes are, respectively, stable and unstable manifolds of the fixed point at the origin.

invariant manifold for the deterministic system. Statistically, the dynamics is symmetric. In particular, we focus on the fraction of the number of bursts with $x<0$ compared with those with $x>0$; with statistical symmetry these are equal. In the physical system motivating this work, the processes we model as noise have a much shorter correlation time than the processes described by the deterministic equations (1) and (2); hence modeling them as noise is appropriate. Noise-stabilized systems are interesting for several reasons. Most importantly, although they can exhibit dynamical behavior that is reminiscent of deterministic chaos, it is likely that their behavior for very low noise level is distinguishable from deterministic autonomous low-dimensional systems. Our model system was chosen to emphasize the noise-stabilizing effect, in the sense that it has no attractor in the zero-noise limit. In physical applications, distinguishing noise-stabilized behavior from more familiar types of dynamics could be critical for understanding and predicting how the system under study will change as the noise driving is modified.

There have been several related papers on nonlinear stochastic equations which are sensitive to a small amount of noise. Sigeti and Horsthemke [5] studied the effect of noise at a saddle-node bifurcation, and found noise-induced oscillations at a characteristic frequency. Stone and Holmes [6] studied systems with an attracting homoclinic orbit or an attracting heteroclinic cycle (structurally stable because of the presence of a symmetry) in the presence of noise. They found that the effect of the noise is to prevent the time between bursts from increasing on each cycle. Lythe and Proctor [7] found that in a system with a slow invariant manifold subject to a fast time scale instability, the system is extremely sensitive to noise. Stone and Armbruster [8] studied structurally stable (again because of symmetry) heteroclinic cycles in the presence of noise, and analyzed the jumping between invariant subspaces of the deterministic system. Armbruster and Stone [9] studied heteroclinic networks in the presence of noise, and the induced switching between cycles. References [6,8,9] stressed the importance of the linear part of the flow near the saddles. Moehlis [10] has investigated a system representing binary fluid convection, and found that states with large bursts can be very sensitive to noise. References [11,12] deal with a system (susceptible-exposed-infected-recovered) describing epidemic outbreaks and show that chaos can be induced for parameters far from the region for which the deterministic system is chaotic.

Our model is different from the above in the following ways: it is motivated by a physical system in which the amplitudes of the bursts, which were not treated in the above references, are important; further, we present experimental results on a circuit, in which the effects of weak symmetry breaking were first observed.

In Sec. II we introduce the deterministic form of the model, and discuss the bursting behavior and the choice of the parameter ν.

In Sec. III we introduce the stochastic model and present results. These results include those on the distribution of maxima of $|x|$ and the time interval T between bursts, and the dependence of these quantities on the noise diffusion coefficient D. A brief discussion of the behavior near the y axis is shown. In this limit, the behavior in x is linear and can be treated by the Fokker-Planck equation, discussed briefly in Appendix A.

In Sec. IV we discuss the role of reflection symmetry in x and the effect of weak symmetry breaking (offset); we show that in a sense the system with noise is structurally stable. We also discuss briefly some modifications to the system at small and large y, and a modified form of the equations in which the noise is replaced by a sinusoidal perturbation.

In Sec. V we show results from an experiment with a nonlinear circuit modeled by Eqs. (1) and (2), showing noise stabilization in a physical system.

In Sec. VI we summarize our work.

II. DETERMINISTIC MODEL

The deterministic form of the model we study is Eqs. (1) and (2). The parameters ϵ, ν are the only parameters that cannot be removed by rescaling x, y, and t. Starting with $x=0$ and $y>0$, y increases in time, going to infinity in finite time if $\nu>1$. For $y>1$ small initial values of x begin to grow. [The instantaneous growth rate of x in Eq. (1) equals $y-1$.] If x grows at a rapid enough rate relative to y (to be quantified later), the second term in Eq. (2) eventually dominates the first and y decreases.

For $\nu>1$ the system has fixed points at $y=1$, $x=\pm x_0$ and at $x=y=0$. Near these fixed points, orbits evolve according to

$$\frac{d}{dt}\delta\mathbf{x}(t)=\mathsf{J}\,\delta\mathbf{x}(t), \tag{3}$$

with

$$\mathsf{J}(x,y)=\begin{bmatrix} y-1 & x \\ -2xy & \epsilon\nu y^{\nu-1}-x^2 \end{bmatrix}.$$

The two fixed points at $x=\pm x_0$, $y=1$ are unstable spirals for

$$0<\nu-1<\sqrt{8/\epsilon}. \tag{4}$$

Orbits continue to spiral outward nonlinearly for $\nu > 1$. This is demonstrated by showing that the function $H(x,y) = y - \ln y + x^2/2 - \epsilon \ln x$ is a Lyapunov function. Indeed,

$$\frac{dH}{dt} = \frac{dx}{dt}\frac{\partial H}{\partial x} + \frac{dy}{dt}\frac{\partial H}{\partial y} = \epsilon(y-1)(y^{\nu-1}-1),$$

so that for $\nu > 1$, $dH/dt > 0$ and the orbits spiral outward for all time, since H has a minimum at $x = x_0$, $y = 1$. For $\nu < 1$, $dH/dt < 0$ and the orbits spiral in to the fixed point. (For $\nu = 1$ the system is equivalent to the Lotka-Volterra system, with Hamiltonian H.)

The system has another fixed point, but with nonanalytic behavior in y for noninteger ν, at $x = 0$, $y = 0$. The axes $x = 0$, $y = 0$ are invariant manifolds; we consider only $y > 0$, and for the noise-free case orbits with $x(0) > 0$ remain in that quadrant. In the range of ϵ and ν given in Eq. (4), orbits spiral away from the fixed points at $(\pm x_0, 1)$ (Fig. 1), approaching the x and y axes, as shown in Fig. 2, which has $\epsilon = 0.5$, $\nu = 1.2$. After an initial transient, the motion is bursty, with each successive oscillation coming closer to the axes, leading to a larger interburst interval, followed by a larger burst.

Next, we turn to a discussion of the choice of the parameter ν. Let us investigate the range of the parameters ν, ϵ for which the system exhibits successively larger and more widely separated bursts.

Consider Eqs. (1) and (2) for large y and small x, i.e.,

$$\frac{dx}{dt} = yx, \tag{5}$$

$$\frac{dy}{dt} = g(0,y) \approx \epsilon y^{\nu}. \tag{6}$$

From these we conclude

$$x = x_c \exp\left(\frac{y^{2-\nu}}{\epsilon(2-\nu)}\right), \tag{7}$$

where $x_c \exp[1/\epsilon(2-\nu)]$ is the value of x when the orbit passes $y = 1$ with small x. Let us compare the two terms on the right in Eq. (2). For $1 < \nu < 2$, the nullcline $dy/dt = 0$ is crossed when $x^2 \geqslant \epsilon y^{\nu-1}$ or

$$x_c^2 \exp\left(\frac{2y^{2-\nu}}{\epsilon(2-\nu)}\right) \geqslant \epsilon y^{\nu-1}, \tag{8}$$

which occurs eventually. So, in each burst, y reaches a maximum and begins to decrease, starting a new cycle, as long as $x \neq 0$. (The orbits with $x = 0$ go to infinity in finite time for $\nu > 1$.)

For $\nu = 2$, we can use Eq. (5) with Eq. (2) for arbitrary x (including the term $-x^2 y$) to obtain, for large y,

$$\frac{dy}{dx} = \epsilon\frac{y}{x} - x.$$

The solution is $y = \zeta x^{\epsilon} - x^2/(2-\epsilon)$, with $\zeta > 0$; the nullcline has $y = x^2/\epsilon$. For $\epsilon < 2$, the nullcline is crossed and the cycle begins again. For $\epsilon > 2$ the nullcline is not crossed and the orbit can go off to infinity in one cycle, in finite time.

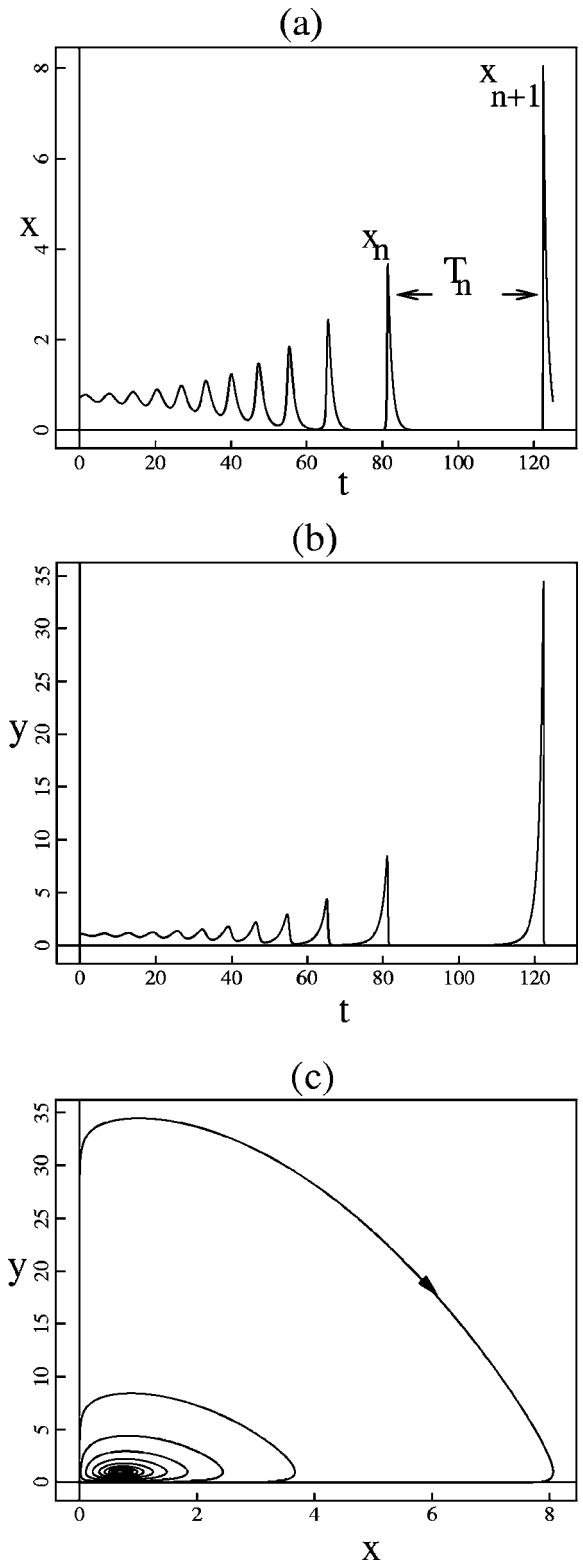

FIG. 2. Orbits (a) $x(t)$ and (b) $y(t)$, and (c) phase plane $y(x)$ for the deterministic equations (1) and (2), with $\epsilon = 0.5$, $\nu = 1.2$, with an initial condition near the fixed point at $x = \sqrt{\epsilon}$, $y = 1$. The orbit spirals out of the fixed point, continuing to expand, eventually piling up near the invariant manifolds $x = 0$, $y = 0$, with bursts to large values of x and y and long interburst time intervals spent mostly near $x = y = 0$.

For $\nu > 2$, the nullcline in Eq. (8) is never reached if x_c is small enough. This means that if the value of x when the orbit crosses $y=1$ is below some critical value, the orbit will go off to infinity before another cycle. Therefore, an orbit starting near the fixed point $(x,y)=(\sqrt{\epsilon},1)$ will encircle the fixed point a finite number of times and then go off to infinity in finite time.

III. STOCHASTIC MODEL AND RESULTS

A. Model

With noise, the system based on Eqs. (1) and (2) is a nonlinear stochastic ordinary differential equation (ODE), of the form

$$\frac{dx}{dt} = f(x,y) + \sqrt{2D}\xi(t), \tag{9}$$

$$\frac{dy}{dt} = g(x,y), \tag{10}$$

with $\xi(t)$ representing uncorrelated unit-variance Gaussian noise, having $\langle \xi(t) \rangle = 0$, $\langle \xi(t)\xi(t') \rangle = \delta(t-t')$. Here, D is the Brownian diffusion coefficient. For a low noise level, $\xi(t)$ affects the dynamics only near the y axis, where $f(x,y)$ is small. The motivation for including noise in the x equation but not in the y equation is the following. Without noise, on the y axis for $y<1$, the magnetic field perturbation $x(t)$ can decrease to an unrealistically low level. Noise prevents x from becoming so small for $0<y<1$, and therefore is expected to prevent the successive bursts from continuing to increase in magnitude, with increasing interburst time interval. We do not include noise in the y equation (the equation for the pressure gradient) because y is a mean field quantity representing mean pressure gradient, which is expected to be much less susceptible to noise. In particular, it would be unphysical for noise to cause the mean pressure gradient y to become negative when the orbit is near the x axis.

We integrate the nonlinear stochastic ODE system (9) and (10) numerically, with a noise term in x added at each time step. Specifically, the time stepping from t to $t+h$ is

$$x(t+h) = x(t) + hf\left(\frac{x(t)+x(t+h)}{2}, \frac{y(t)+y(t+h)}{2}\right) + \sqrt{2Dh}\xi(t),$$

$$y(t+h) = y(t) + hg\left(\frac{x(t)+x(t+h)}{2}, \frac{y(t)+y(t+h)}{2}\right). \tag{11}$$

The implicit form of the deterministic part is solved by a simple Picard iteration, and the random term is added. Each value $\xi(t)$ is an independent random number with zero-mean Gaussian distribution and unit variance, and the coefficient $\sqrt{2Dh}$ is chosen to give results independent of h (in a mean square sense) for small h.

B. Numerical results

Results for the same parameters as in Fig. 2, with noise having $D=5\times10^{-9}$, are shown in Fig. 3, with $0 \leqslant t \leqslant 1000$. The orbits are still of a bursty nature, but the bursts and the interburst time intervals are limited in magnitude. The successive bursts appear to be uncorrelated and bursts with x negative are as common as those with x positive, after the transient near the fixed point at $x=x_0=\sqrt{\epsilon}$, $y=1$. To the eye, these results appear similar to those of a chaotic deterministic system, e.g., the y-z projection of the Lorenz system [13].

To analyze the bursts in terms of amplitude and time interval between bursts, we introduce x_n, x_{n+1} and T_n (see Fig. 2). These are, respectively, the amplitude (in x) of a burst (a local maximum for positive x, a local minimum for negative x), the amplitude of the following burst, and the time interval between them. In Fig. 4 we show scatter plots of T_n vs x_n, x_{n+1} vs T_n, and the composite x_{n+1} vs x_n for the parameters of the case of Figs. 3 and 4, indicating the probability density functions $f_1(x_n,T_n)$, $f_2(T_n,x_{n+1})$, and $f_3(x_n,x_{n+1})$. These are the marginal distributions of the full distribution $g(x_n,T_n,x_{n+1})$ projected over x_{n+1}, x_n, and T_n, respectively. The first has very little scatter. This property is related to two aspects. One is the fact that the noise is added only to $x(t)$ and has little effect except when x is small. The other is that most of the time interval T_n is spent near the saddle at $x=y=0$, after the burst but before the orbit can be influenced again by the noise, as it passes along the y axis near $y=1$. This lack of scatter shows a very strong correlation. However, this correlation is strongly nonlinear and would not be reflected in the linear correlation coefficient, but would require a diagnostic such as the conditional entropy [14]. The other plots show the expected symmetry in x. Specifically, there are four equivalent peaks in the four quadrants in Fig. 4(c), showing that successive peaks are positive or negative, independent of the sign of the previous peak. Figure 4(b) shows a long tail in T_n, and sharp cutoffs for small $|x_n|$ and small T_n.

In Fig. 5 are histograms, showing the marginal distributions of x_n, at the maxima of $|x|$, and the interburst time T_n. (See Fig. 2.) The maximum time was $t=10^6$ and there were about 23 000 peaks in x_n and the same number of interburst intervals T_n. The histogram of x_n is symmetric and shows peaks at $|x_n|=3.7$, with tails around $|x_n|=4.5$ and a sharp cutoff inside at $|x_n|=3.3$. The latter histogram, reflecting the nonlinear correlation of T_n with x_n shown in Fig. 5(a), has a strong cutoff inside $T_n=30$, a peak at $T_n=38$, and a tail for $T \sim 60-80$.

Based on Sec. II, we expect considerably different results for $\nu > 2$. These results show that, for the deterministic system, if the value of x at the *throat* $y=1$ is small enough, the orbit will go off to infinity before another cycle occurs. Therefore, we expect that if the noise level D is small enough, the orbit may have a few bursts, but will diverge to infinity as soon as the cycle comes close enough to $x=0$ as it crosses $y=1$. For large values of D, the orbit may behave as in Fig. 3 for a very long time, but whenever x becomes small enough at the inner crossing of $y=1$, the orbit will also go to infinity before another cycle. Numerical simulations bear this out.

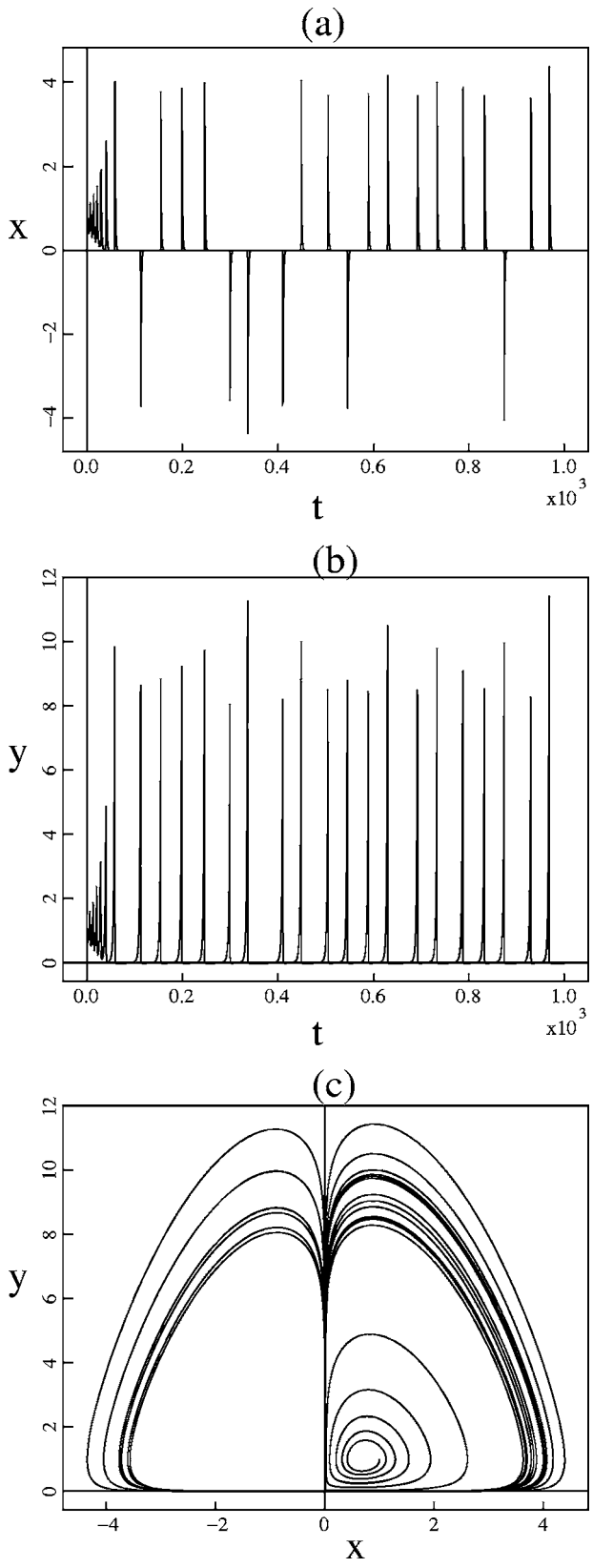

FIG. 3. Orbits (a) $x(t)$, (b) $y(t)$, and (c) phase plane y vs x for the system with noise, Eqs. (9) and (10). The parameters are equal to those in Fig. 2, with $D=5\times10^{-9}$. The initial condition is near the spiraling fixed point, so that the transient spiral shows. Note that the maximum time $t=10^3$ is much larger than in Fig. 2.

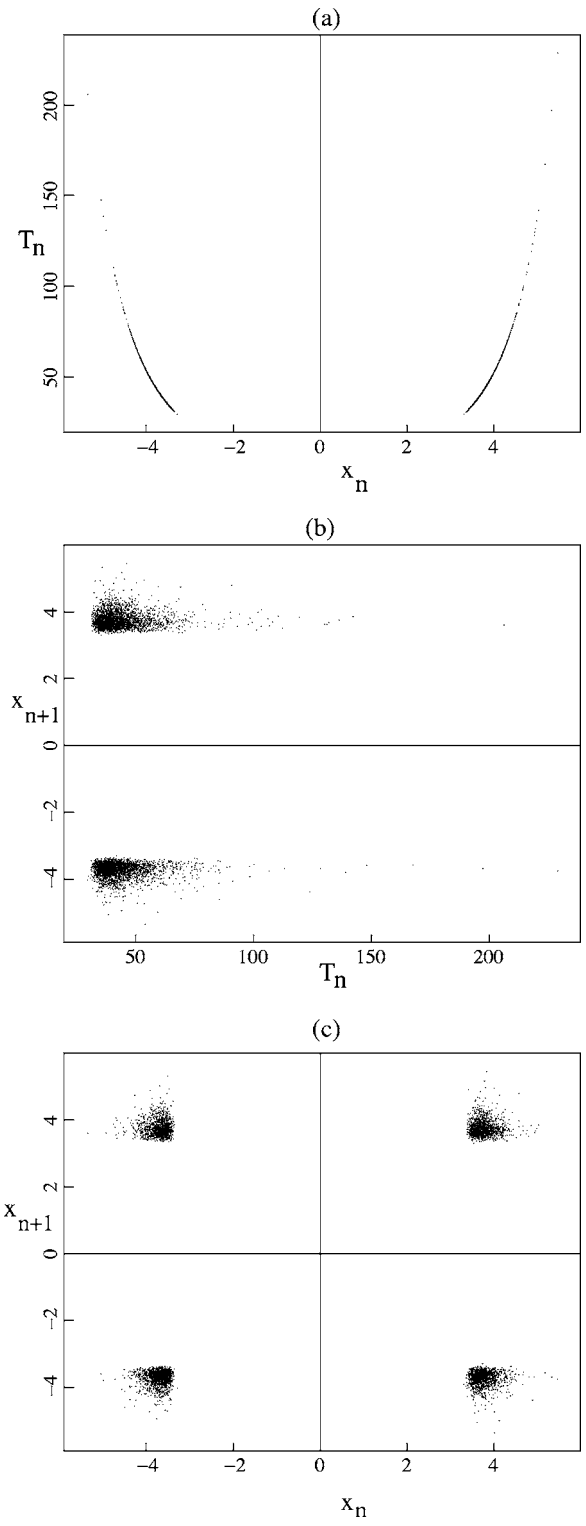

FIG. 4. Scatter plots (a) T_n vs x_n, (b) x_{n+1} vs T_n, and (c) x_{n+1} vs x_n for the case of Fig. 3. Note that there is hardly any scatter in (a). The extent of the burst [measured as $|x_n|$ or as the peak of $y(t)$] determines T_n, because after a larger burst the orbit approaches the origin closer to the x axis, because most of the interburst time is spent near $x=y=0$, and because the noise is effective only near the y axis. The statistics plotted in (b) is symmetric in x_{n+1} and has a long tail in T_n. The plot in (c) is symmetric in x_n and x_{n+1}, with four essentially identical peaks near $|x_n|=|x_{n+1}|=4$.

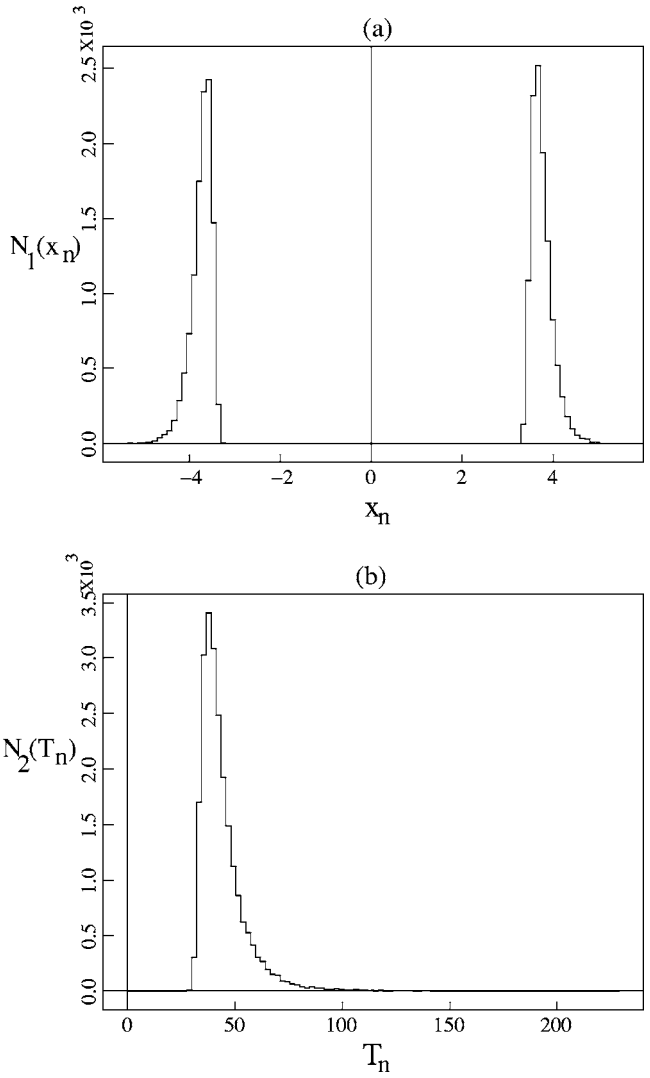

FIG. 5. Histograms $N_1(x_n)$, $N_2(T_n)$ of (a) x_n, extrema of x, and (b) time intervals T_n, respectively, showing the marginal distributions for these quantities. The histogram of $|x_n|$ in (a) has a tail with $|x_n| \gtrsim 5$ and a strong cutoff for $|x_n| < 3.3$; T_n in (b) also has a tail to the right and a sharp cutoff to the left. For this case the mean values are $\langle |x_n| \rangle = 3.87$ and $\langle T_n \rangle = 49.1$, respectively.

C. Fokker-Planck analysis near $x=0$

The maxima in $|x|$ occur at $y=1$. These are related to the values of x near zero for which $y=1$: for small values of D, the noise is important only near the y axis, and as the orbit lifts off this manifold it essentially obeys the deterministic equations, and therefore the peaks in $|x|$ are determined to high accuracy by the crossing of $y=1$ for small x (Fig. 6). In this section we quantify this behavior by means of analysis involving the Fokker-Planck equation for behavior near the y axis.

As the orbit travels near the y axis, $x(t)$ satisfies the linear stochastic equation

$$\frac{dx}{dt} = \gamma(t)x + \sqrt{2D}\xi(t), \tag{12}$$

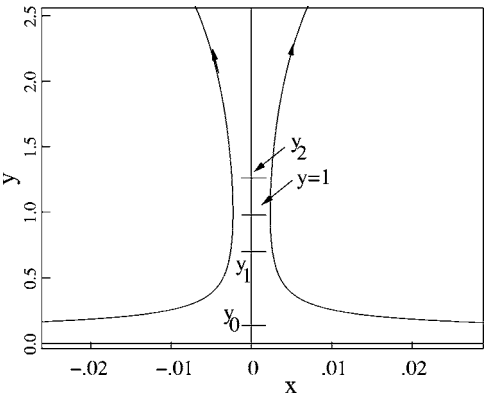

FIG. 6. Sketch of deterministic orbits near $x=0$. The minima of $|x|$ are at the throat $y=1$. In this region, the equations can be linearized with respect to x and noise can have a large influence. The values $y=y_1, 1, y_2$ correspond to $t=t_1, 0, t_2$ in the text.

where $\gamma(t)=y(t)-1$; for small x, y satisfies $\dot{y}=\epsilon y^\nu$, independent of x. The noise $\xi(t)$ has the statistical characteristics described after Eqs. (9) and (10). Linearization in x holds for small D, up to the time when the term $-x^2y$ in Eq. (2) becomes important. For low noise level (small D), the successive bursts are large in magnitude, leading to small values of x on the next pass. On each successive pass near $y=1$, the correlation with the previous peak of $|x|$ is lost. This behavior is due to the fact that for $g(0,y)=\epsilon y^\nu$ with $\nu > 1$, x becomes small enough to become dominated by the noise while $y < 1$.

In Appendix A we have included an analysis based on the Fokker-Planck equation for orbits near $x=0$, where Eq. (12) is valid. Conclusions based on this Fokker-Planck analysis and direct simulations are the following. The mean value $\langle |x_n| \rangle$ [cf. Fig. 5(a)] decreases with D. The dependence of this quantity is shown as a function of D in Fig. 7(a). The mean of the histogram of the interburst time T_n as a function of D is shown in Fig. 7(b). As we discuss in Appendix A, the orbits cross $y=1$ with typical values of x proportional to $\sigma_x \sim \alpha^{1/2} \sim D^{1/2}/\epsilon^{1/4}$, and proceed with little subsequent effect of noise. The dependence of $\langle |x_n| \rangle$ on D appears to be approximately logarithmic for small D.

The analysis in Appendix A shows that for small x, near the intersection with $y=1$, x has a Gaussian distribution $f(x) \propto e^{-x^2/2\sigma_x^2}$. This yields a distribution for x', at the next crossing of $y=1$ where $|x_n|$ is a maximum, equal to

$$g(x') = |dx/dx'| f(x(x')).$$

The second factor is responsible for the sharp cutoff to the left of the peak in x' [Fig. 5(a)], corresponding to x being in the tail of the Gaussian. The tail to the right of the peak in Fig. 5(a) is due to the Jacobian factor $|dx/dx'|$. From the Gaussian form for $f(x)$ we obtain $|dx/dx'| \sim x' e^{-x'^2}$ and

$$g(x') \propto (x' e^{-x'^2}) e^{-x(x')^2/2\sigma_x^2}.$$

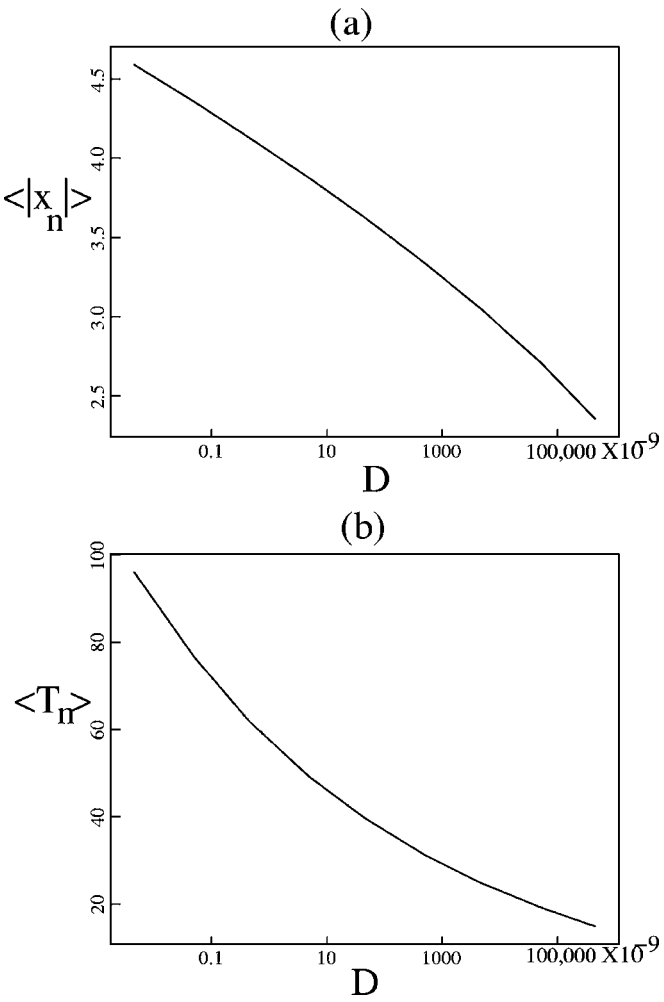

FIG. 7. Mean values of (a) the burst peaks $\langle|x_n|\rangle$ and (b) the interburst time $\langle T_n\rangle$ as functions of D. The parameters (except for noise level) are the same as in Fig. 2. The quantity $\langle|x_n|\rangle$ appears to behave logarithmically for small D.

The first (Jacobian) factor $x'e^{-x'^2}$ gives a Gaussian-like tail for large x' and the second factor gives a cutoff for x' close to the fixed point $x'=x_0=\sqrt{\epsilon}$, where $x'-x_0=-s_1(x-x_0)$. This cutoff is sharp if $\sigma_x \ll x_0$.

IV. THE ROLE OF SYMMETRY AND RELATION WITH OTHER MODELS

We have commented that the system (9) and (10) has certain features that are not generic. These issues are (a) the fact that deterministic orbits eventually go to infinity, (b) the nonanalytic behavior of y^ν near $y=0$, and (c) the reflection symmetry of the equations in x. To deal with issue (a), we have considered a system with $\epsilon y^\nu \to \epsilon y^\nu(1-\eta y)$ in Eq. (2). For small enough η or large enough noise level, the orbits stay well below the new fixed point at $x=0$, $y=1/\eta$ and the results are essentially identical to those with $\eta=0$. Regarding issue (b), we considered modified systems without the dominant y^ν behavior at $y=0$, e.g., $\epsilon y^\nu \to \epsilon(\beta y+y^\nu)$. The results are essentially identical to those of Sec. III B, with the exception that the time intervals between bursts are typically shorter for $\beta>0$. We deal with issue (c) in Sec. IV A.

Also, we have integrated Eqs. (1) and (2) with a sinusoidal term $\xi(t)=b\sin(\omega t)$ added to the x equation rather than random noise. The sinusoidal and random forms of $\xi(t)$ are extremes of temporal driving, with quasiperiodic time dependence and colored random time dependence as intermediate cases. In all such cases the analysis of Sec. III B indicates that the typical value of x at $y=y_2$ is the important factor. (See Sec. III B and Fig. 6.) To explore this further, we have obtained results for $\nu=1.2$, $\epsilon=0.5$, as in Fig. 3, and with various values of ω and b. The results were found to be qualitatively similar to those with noise, with a simple relation between b and D, showing that indeed the accumulated effect on x at the time $y=y_2$ is the determining factor. That is, $\sigma_x \sim b/\omega$ or $b/\omega \sim D^{1/2}/\epsilon^{1/4}$. In particular, the behavior of $\langle|x_n|\rangle$ and $\langle T_n\rangle$ are similar. [Also, we have computed the Lyapunov exponent h_1 for the case with $\xi(t)$ random as well as sinusoidal. For $\sigma_x \sim b/\omega$, h_1 is comparable.]

A. Breaking of the symmetry in x

We have investigated the effect of breaking the reflection symmetry $x \to -x$ in Eqs. (9) and (10), motivated by the experimental results shown in Sec. V. The simplest way of breaking this symmetry is to introduce a constant offset. With this offset, Eq. (9) takes the form

$$\frac{dx}{dt} = (y-1)x + a + \sqrt{2D}\xi(t), \tag{13}$$

with the y equation unchanged. With zero noise and for $a>0$ a stable limit cycle is formed to the right of $x=0$, and points near $(x,y)=(0,0)$ go into this limit cycle. (For $a<0$ the results are identical, with $x \to -x$.) Therefore the zero-noise results of Sec. II are not structurally stable with respect to such an offset.

However, in the presence of noise, the results change considerably. In Figs. 8(a) and 8(b) we show $x(t)$ and the phase portrait y vs x for a case with the same parameters as in Fig. 3 (in particular with $D=5\times10^{-9}$), but with $a=5\times10^{-5}$. The results are qualitatively similar to those in Fig. 3 except that most of the bursts go to the right. In Fig. 8(c) we show the fraction Φ of bursts that go to the left as a function of the offset a for three values of D. For $a \lesssim \sqrt{D}$, the fraction Φ is appreciable and the orbits behave qualitatively as in Fig. 3. For $a \gtrsim \sqrt{D}$, on the other hand, virtually all the orbits go to the right ($\Phi \approx 0$) and therefore behave qualitatively as the limit cycle found for $D=0$, $a>0$. These results, and those of Appendix A showing $\sigma_x \sim \sqrt{D}$, indicate that the offset changes the results qualitatively if it moves the orbit outside the region near $x=0$ where noise dominates.

This brings up the issue of structural stability of the behavior observed for $a=0$. For zero noise, this behavior, seen in Fig. 2, is certainly not structurally stable. However, for $D>0$ the qualitative behavior persists as long as $a \lesssim \sqrt{D}$. (For small x, this conclusion is consistent with the scaling

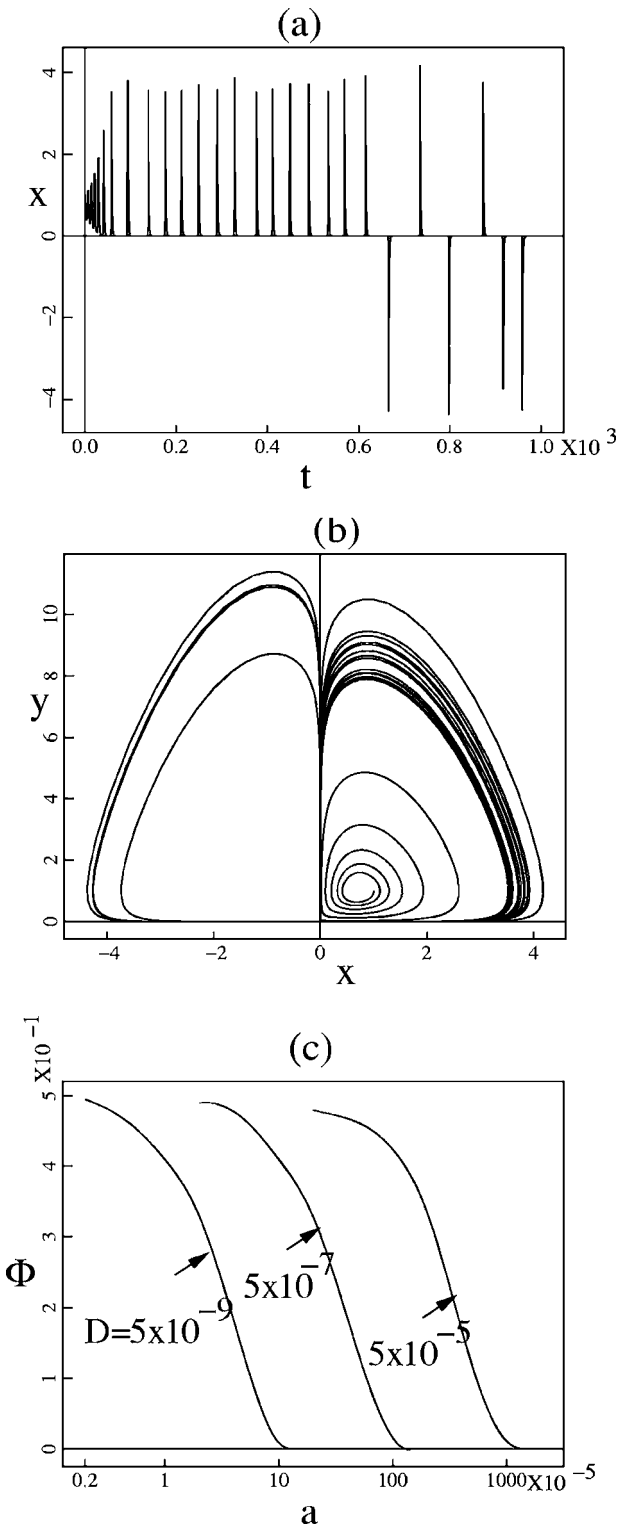

FIG. 8. Results with an offset [cf. a in Eq. (13)]. In (a) and (b) are $x(t)$ and y vs x for parameters as in Fig. 2, again with $D=5\times10^{-9}$. In (c) is the fraction Φ of bursts to the left, for three values $D=5\times10^{-9}$, 5×10^{-7}, 5×10^{-5}.

symmetry $x\to\lambda x$, $a\to\lambda a$, $D\to\lambda^2 D$.) In this modified sense, the system with finite noise is structurally stable.

We will return to the issue of an offset in the electronic circuit in the next section.

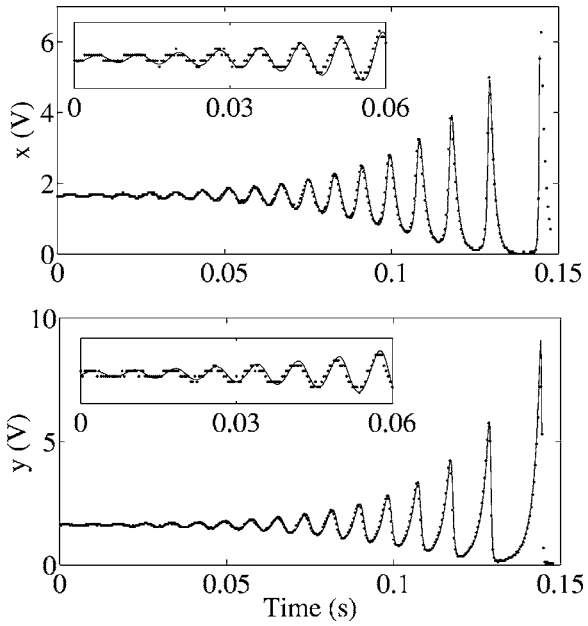

FIG. 9. Circuit output (dots) compared to numerical solution of the ODE (traces), with parameters as in Fig. 2. Adjusting the simulation parameters to fit the data showed that all circuit parameters are within 3% of their expected values. The insets show the agreement of the (digitized) data and simulation near the fixed point.

V. ELECTRONIC CIRCUIT

In order to test for noise stabilization in a physical system, we have constructed a circuit which integrates Eqs. (9) and (10). In dimensionless integral form, these equations are $x(\tau)=x_0+\int_{\tau_0}^{\tau}[(y-1)x+\hat{\xi}(\tau')]d\tau'$ and $y(\tau)=y_0+\int_{\tau_0}^{\tau}(\epsilon y^{\nu}-x^2 y)d\tau'$, and the parameter values used in the circuit were $\epsilon=0.5$ and $\nu=1.2$, as in Figs. 3–5, 7, and 8. The circuit design is shown in Fig. 12 below. The white noise, $\hat{\xi}(t)=\sqrt{2D}\xi(t)$, stabilized the oscillations, and Figs. 9–11 show that the circuit output agreed well with numerical solution of Eqs. (12) and (13). We also observed the structural instability in these equations. See Appendix B for a description of the circuit design.

A. Properties of the added noise

The noise was generated by creating random numbers and recording them to a .wav file to play back via the computer's audio output at the standard rate of 44 kHz. This net process effectively filters the noise through a low-pass filter. When we sampled the noise using a digital oscilloscope, we found that the noise had a relatively constant spectrum to frequencies as high as 20 kHz. We autocorrelated the noise, and found that it was well represented by

$$\langle V_N(t)V_N(t')\rangle = \frac{A_0}{\pi(t-t')}\sin 2\pi\frac{(t-t')}{T}$$

with a period $T=50$ μs, which also represents a flat spectrum filtered by a 20 kHz low-pass filter. For times longer than $T/(2\pi)$, this autocorrelation function is a good approxima-

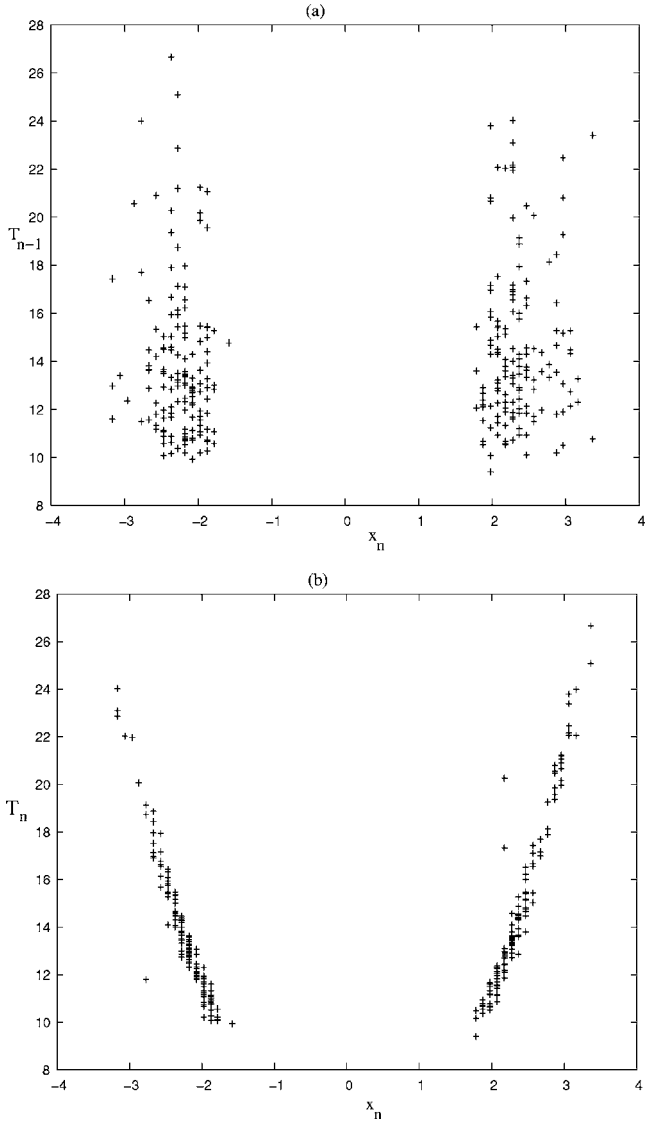

FIG. 10. Comparison of peak height x_n to (a) time since previous peak T_{n-1} and (b) time until next peak T_n, from experiments. The correlations seen here are indicative of noise stabilization. The noise level is $D \simeq 4.7 \times 10^{-4}$.

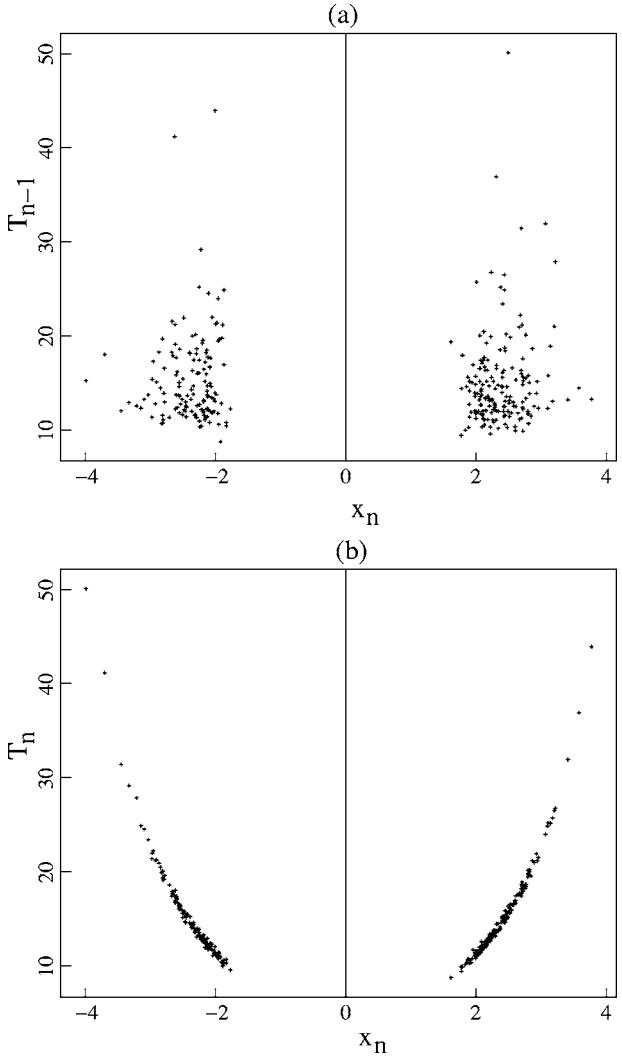

FIG. 11. The same quantities as in Fig. 10 from numerical computation of Eqs. (9) and (10).

tion of $A_0\delta(t)$. By evaluating the autocorrelation function at $t=0$, we can determine that $A_0=(T/2)\langle V_N^2\rangle$ so the diffusion rate is $A_0/2$ or

$$D = \left\langle \left(\frac{V_N}{V_2}\right)^2 \right\rangle \left(\frac{R_2}{R_4}\right)^2 \frac{T}{4R_1C_1}$$

in terms of the scaled variables used in Appendix B. The theoretical minimum diffusion constant for our circuit parameters given by Eq. (B1) is well below the intrinsic noise in the circuit. This intrinsic noise is not well characterized and occurs in both the x and y variables. We use a large enough value of the noise amplitude so that the intrinsic noise contribution is negligible. We show in Figs. 10 and 11 the quantities T_{n-1} vs x_n and T_n vs x_n, first obtained from the experiment and also by integrating numerically the differential equations with the same parameters, in particular $D=4.7\times10^{-4}$. (These results are similar to those in Fig. 4, but with a different value of D.) The agreement is very good.

B. Offsets and symmetry breaking

The primary difficulty in designing this circuit is that small DC offsets at the input of the integrators significantly change the differential equations. In particular, an offset in the input to the y integrator either drives the V_y output negative to create an error in the AD538 computational unit, or it leads to a stable limit cycle similar to that described in Sec. IV. We adjusted a small current ($\sim$0.45 μA) to minimize the V_y offset, using the automatic reset circuit to recover whenever V_y became negative. The reset kicks the circuit back into the vicinity of one of the unstable spirals. The x integrator naturally follows, bringing V_x to a value near its fixed point. Without this reset, a negative value of V_y leading to the failure of the AD538 causes the circuit to fall to a stable fixed point with a large negative value of V_y. An external trigger can also reset the circuit to values near its unstable fixed point.

Similarly, we also corrected the offset in the x integrator by adding $\sim 0.2\ \mu$A at the integrator input. We adjusted this value until the noise signal generated equal numbers of negative and positive x pulses. After these adjustments, we observed the basic structure of the oscillations as they evolved away from the fixed point, in order to verify that the circuit wave forms were the same as the model calculations (see Fig. 9). The fact that such a simple adjustment can give results in agreement with the symmetric model is consistent with the extended concept of structural stability discussed at the end of Sec. IV A. The results also show that the circuit is a sensitive detector of offsets.

VI. SUMMARY

We have performed a study of a nonlinear stochastic ODE whose deterministic form has unstable spirals, leading to bursty behavior, with successive bursts growing in magnitude and with larger time intervals between them. This bursty behavior is due to the fact that after each burst, the orbit comes closer to the unstable manifold (y axis) of a hyperbolic fixed point at the origin, and therefore travels farther along this unstable manifold before diverging from it to form the next burst.

In the presence of noise at a very small level, the bursts get stabilized in the sense of becoming limited in magnitude. The time interval between them is also limited, and the bursts can go to either positive or negative x. In many qualitative senses, the behavior appears like deterministic chaos.

This system has reflection symmetry in x; an offset a in x destroying this symmetry can lead to completely different behavior, depending on its magnitude relative to the noise. That is, the bursty behavior seen in the symmetric deterministic equations is not structurally stable. With noise and a small value of the offset $|a| < \sqrt{2D}$ (D is the Brownian diffusion coefficient), the bounded bursty behavior persists, but with more bursts going to the right if $a > 0$ (to the left if $a < 0$.) For larger offset $a \gtrsim \sqrt{2D}$, all bursts go to the right and basically give a noisy form of the stable limit cycle. In this sense, the results in the presence of noise and $a = 0$ are structurally stable.

We have described briefly results on a nonlinear circuit satisfying the same equations as the model. The circuit behaves similarly to the model. In particular, the circuit is very sensitive to the presence of an offset, and in practice the offset is adjusted to minimize the asymmetry of the signal. More details are presented in Ref. [15] and in Appendix B.

The system (9) and (10) and its generalizations in Sec. IV are arguably the simplest realizations of systems in which a small noise level can limit the amplitude of bursts and lead to qualitatively distinct behavior. We have listed in the Introduction physical examples of systems in which this effect may be important. For the tokamak example, the results here should have an impact on low-dimensional modeling of ELMs. Indeed, the observation of chaotic time dependence of ELM data suggests that a simple autonomous ODE model must be three dimensional. However, tokamaks are known to have a broad spectrum of fluctuations (turbulence). If these fluctuations can be treated as uncorrelated noise, i.e., if their correlation time is much shorter than ELM time scales, it is justifiable to explore two-dimensional models with noise such as the models studied here.

ACKNOWLEDGMENTS

We wish to thank C. Doering, J. Guckenheimer, E. Ott, and D. Sigeti for valuable discussions. This work was supported by the U.S. Department of Energy, under Contract No. W-7405-ENG-36, Office of Science, Office of Fusion Energy Sciences, and by the NSF-DOE Program in Basic Plasma Physics under Contract No. PHY-0317256.

APPENDIX A: FOKKER-PLANCK EQUATION

The stochastic behavior of Eq. (12) is governed by the Fokker-Planck equation for the probability density function $f(x,t)$,

$$\frac{\partial f}{\partial t} + \frac{\partial}{\partial x}[\gamma(t) x f] = \frac{\partial}{\partial x}\left(D \frac{\partial f}{\partial x}\right), \tag{A1}$$

where $D = \sigma^2/2$ is the diffusion coefficient. For arbitrary $\gamma(t)$, Eq. (A1) has the exact solution

$$f(x,t) = \sqrt{\frac{1}{2\pi\alpha(t)}}\, e^{-x^2/2\alpha(t)}$$

with $d\alpha/dt = 2[\alpha(t)\gamma(t) + D]$. This has the solution

$$\alpha(t) = 2D \int_{-\infty}^{t} ds_1 \exp\left(2\int_{s_1}^{t} \gamma(s_2) ds_2\right),$$

assuming $\alpha(t \to -\infty) = 0$. Thus, $\alpha(t)$ is proportional to D, with a coefficient depending on $\gamma(t)$.

If γ is approximately constant ($|\dot{\gamma}/\gamma^2| \ll 1$) and negative, we obtain

$$f(x,t) \to \sqrt{|\gamma(t)|/2\pi D}\, e^{-|\gamma(t)| x^2/2D}. \tag{A2}$$

Another regime, entered at $t = t_1$, is found by neglecting $\gamma(t)$ in Eq. (A1), giving the purely diffusive random walk result

$$f(x,t) \sim \frac{1}{\sqrt{4\pi(Dt + \alpha_0)}}\, e^{-x^2/4(Dt+\alpha_0)}. \tag{A3}$$

A third range has γ positive with advection dominating diffusion. We find

$$\alpha(t) = \alpha(t_2) \exp\left(2\int_{t_2}^{t} \gamma(s) ds\right), \tag{A4}$$

where t_2 is the time this range is entered, i.e., where $\gamma(t_2)\alpha(t_2) \sim D$. In this range the noise becomes negligible.

For application to Eqs. (9) and (10), consider x small so that its equation is linear [when the second term on the right in Eq. (10) is negligible]. We then note that if α is small for $y \approx 0$, then $\alpha(t)$ near $y = 1$ [recall $\gamma(t) = y(t) - 1 = 0$] is proportional to $D/\sqrt{\dot{\gamma}_0}$. Since $\dot{\gamma} = \dot{y} \sim \epsilon$, we have $\alpha(y \approx 1) \sim D/\sqrt{\epsilon}$. After a diffusive stage ($t_1 < t < t_2$, $y_1 < y < y_2$), α continues to increase as in Eq. (A4), with noise no longer playing a

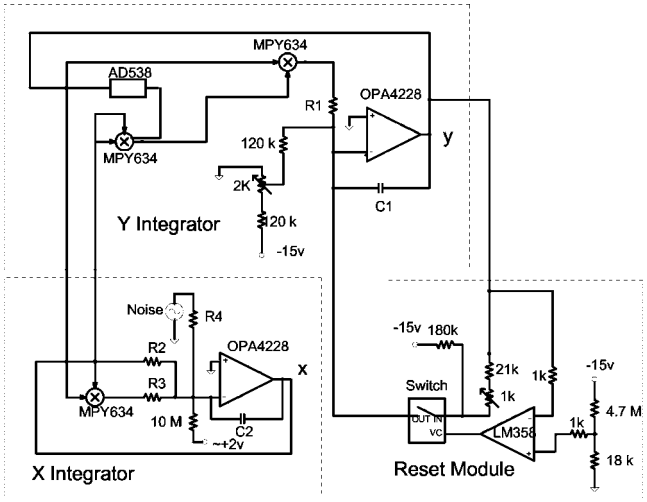

FIG. 12. Circuit diagram.

role. Thus, the nonlinear orbit for later times depends only on the noise accumulated by the time (here $t=t_2$, $y=y_2$); the value of x at $y\approx y_2$, when noise last plays a role, is proportional to $\sqrt{\alpha}\propto D^{1/2}/\epsilon^{1/4}$. See Fig. 6. Thus, in essence, the orbit from the crossing of $y=1$ with small x out to the next crossing and back to near the origin is deterministic, and the noise plays its role only along the y axis.

APPENDIX B: CIRCUIT DESIGN

The design of our circuit is basically the same as reported in Ref. [15], but we have adjusted our circuit parameters, and extended the analysis of the circuit behavior. For the sake of completeness, we have included all of the new circuit parameters in this appendix, as well as our analysis of the minimum noise amplitude necessary to keep the circuit from saturating the circuit elements.

The analog circuit consists of three basic subcircuits: the x integrator, the y integrator, and the reset controller, as shown in Fig. 12. The integrators use OPA 4228 operational amplifiers (low noise, 33 MHz bandwidth) with capacitive feedback (10 nF) to integrate their inputs. V_1 and V_2 are constant applied voltages, while V_x and V_y are time-varying voltages, proportional to $x(\tau)$ and $y(\tau)$, respectively.

The input to the y integrator uses an AD538 real-time computational unit (400 kHz bandwidth) to raise the V_y voltage to a fractional power $V_y(t)^{\nu-1}$ by taking its logarithm, scaling the result by $\nu-1$, and then exponentiating to generate $V_1[V_y(t)/V_2]^{\nu-1}$. This output is then added into the output of an MPY634 precision multiplier (10 MHz bandwidth) that creates the ratio $V_x^2(t)/V_2$. A second MPY634 multiplies this combined signal by V_y/V_2 before it enters the integrator. We also use additional small adjustable current sources to eliminate offsets.

The input to the x integrator is the sum of V_x, the noise source, and V_xV_y/V_2 formed by another MPY634. The net output signal of the entire circuit has a maximum frequency of 2 kHz, well within the bandwidth limit of all the components. This circuit does the following integrations:

TABLE I. Values of circuit elements.

V_1	0.4 V
V_2	10 V
R_1	6.8 kΩ
R_2	122 kΩ
R_3	19.5 kΩ
R_4	67 kΩ
C_1	10 nF
C_2	10 nF

$$V_x(t) = V_x(t_0) + \int_{t_0}^{t} \left(\frac{R_2 V_y(t')}{R_3 V_2} - 1 \right) V_x(t') \frac{dt'}{R_2 C_2} + \int_{t_0}^{t} V_N(t') \frac{dt'}{R_4 C_2},$$

$$V_y(t) = V_y(t_0) + \int_{t_0}^{t} \left(V_1 \left(\frac{V_y(t')}{V_2} \right)^{\nu} - \left(\frac{V_x(t')}{V_2} \right)^2 V_y(t') \right) \frac{dt'}{R_1 C_1},$$

where the circuit components had the values listed in Table I, and the parameter $\nu-1$ was set to 0.2 in the AD538 component by a voltage divider composed of a 2200 Ω resistor and a 560 Ω resistor. This dimensional form of the equations is related to the dimensionless form by defining x, y, τ, ϵ, and η as

$$y = \frac{R_2}{R_3} \frac{V_y}{V_2},$$

$$\tau = \frac{t}{R_2 C_2},$$

$$\epsilon = \frac{R_2 C_2}{R_1 C_1} \frac{V_1}{V_2} \left(\frac{R_3}{R_2} \right)^{\nu-1},$$

$$x = \sqrt{\frac{R_2 C_2}{R_1 C_1}} \frac{V_x}{V_2} = \sqrt{\epsilon} \frac{V_x}{\sqrt{V_1 V_2}} \left(\frac{R_2}{R_3} \right)^{(\nu-1)/2},$$

$$\eta = \sqrt{\frac{R_2 C_2}{R_1 C_1}} \frac{V_N}{V_2} \frac{R_2}{R_4}.$$

This leads to fixed points at

$$V_{y^*} = \frac{R_3}{R_2} V_2,$$

$$V_{x^*} = \sqrt{V_1 V_2} \left(\frac{R_3}{R_2} \right)^{(\nu-1)/2}.$$

Thus, a circuit design with a given value of ϵ has its fixed points and its voltage scaling determined by the choice of the ratio R_3/R_2. This value can be optimally set by forcing both the x circuit and the y circuit to reach saturation values on the same cycle. These two peak values cannot require voltages in excess of V_2, or the multipliers will fail, and the peaks will be clipped. To optimize, we equate these peaks

when they reach V_2; for the $\nu=1$ case this gives $\epsilon V_2/V_1 = 2R_2/R_3$ or, for our values of V_1 and V_2,

$$\frac{R_2}{R_3} = \frac{\epsilon}{2}\frac{V_2}{V_1} = 6.25.$$

This choice then implies maximum values of $x_m = \sqrt{2(\epsilon V_2/2V_1)} = 3.53$, and $y_m = \epsilon V_2/2V_1 = 6.25$. These maximum values of x and y determine the minimum noise amplitude that must be present to keep the voltage peaks within the operating range of the multipliers. The logarithmic dependence observed in Fig. 7 can be approximated as $\langle x \rangle = (1/8)\ln(10^5/D)$, so that

$$D_{min} = 10^5 e^{-8x_m} = 10^5 e^{-8\sqrt{2(\epsilon V_2/2V_1)}} \sim 2 \times 10^{-10}. \quad \text{(B1)}$$

When the amplitudes are low enough to avoid clipping, the measured results are in agreement with those given in Sec. III B.

[1] H. Zohm, Plasma Phys. Controlled Fusion **38**, 105 (1996).
[2] J. W. Connor, Plasma Phys. Controlled Fusion **40**, 191 (1998).
[3] X. D. Shi, M. P. Brenner, and S. R. Nagel, Science **265**, 5169 (1994).
[4] C. Liu, R. Roy, H. D. I. Abarbanel, Z. Gills, and K. Nunes, Phys. Rev. E **55**, 6483 (1997).
[5] D. Sigeti and W. Horsthemke, J. Stat. Phys. **54**, 1217 (1989).
[6] E. Stone and P. Holmes, SIAM J. Appl. Math. **50**, 726 (1990).
[7] G. D. Lythe and M. R. E. Proctor, Phys. Rev. E **47**, 3122 (1993).
[8] E. Stone and D. Armbruster, Chaos **9**, 499 (1999).
[9] D. Armbruster, E. Stone, and V. Kirk, Chaos **13**, 71 (2003).
[10] J. Moehlis, Phys. Lett. A **284**, 172 (2001).
[11] L. Billings and I. B. Schwartz, J. Math. Biol. **44**, 31 (2002).
[12] E. M. Bollt, L. Billings, and I. B. Schwartz, Physica D **173**, 153 (2002).
[13] E. Ott, *Chaos in Dynamical Systems* (Cambridge University Press, Cambridge, U.K., 2002).
[14] T. M. Cover and J. A. Thomas, *Elements of Information Theory* (Wiley, New York, 1991).
[15] W. E. Cooke, A. S. Richardson, E. R. Tracy, W. Tang, and J. M. Finn, in *Proceedings of the Eighth Experimental Chaos Conference*, edited by S. Boccaletti, B. Gluckman, J. Kurths, L. Pecora, R. Meucci, and O. Yordanov, AIP Conf. Proc. No. 742 (AIP, Melville, NY, 2004), p. 63.